

# Extended-soft-core baryon-baryon model ESC16. IV. $S = -3$ and $S = -4$ hyperon-hyperon interactions

M. M. Nagels,<sup>1</sup> Th. A. Rijken<sup>1,2,\*</sup> and Y. Yamamoto<sup>2</sup>

<sup>1</sup>*Institute of Mathematics, Astrophysics, and Particle Physics, Radboud University, Nijmegen, The Netherlands*

<sup>2</sup>*Nishina Center for Accelerator-Based Science, Institute for Physical and Chemical Research (RIKEN), Wako, Saitama 351-0198, Japan*



(Received 9 October 2022; revised 11 April 2023; accepted 8 August 2023; published 23 August 2023)

**Background:** This paper presents the extended-soft-core (ESC) potentials ESC16 for baryon-baryon ( $BB$ ) channels with total strangeness  $S = -3$  and  $-4$ . For these channels no experimental scattering data exist, apart from very recently measured preliminary correlations. Also, there is no information from hypernuclei or hyperonic matter.

**Purpose:** The aim is to calculate the predictions of the ESC16 model for the  $S = -3$  and  $S = -4$   $BB$  channels.

**Methods:** The potential models for  $S = -3$  and  $-4$  are based on  $SU(3)$  extensions of potential models for the  $S = 0$  and  $-1$  and  $S = -2$  sectors, which are fitted to experimental data. Flavor  $SU(3)$  symmetry is broken “kinematically” by the masses of the baryons and the mesons. The fit to the  $S = 0$  and  $-1$  sectors provides the necessary constraints to fix all free parameters, i.e., baryon-baryon-meson couplings and cutoff masses. The  $S = -2$  systems are constrained by the  $\Delta B_{\Lambda\Lambda}$  value from the Nagara event and the requirement of  $U_{\Xi} \approx -10$  MeV.

**Results:** Various properties of the potentials are illustrated by giving results for scattering lengths, bound states, and phase parameters.

**Conclusions:** No  $\Xi\Xi$ ,  $\Xi\Lambda$ , and  $\Xi\Sigma$  bound states are predicted by the ESC16 model.

DOI: [10.1103/PhysRevC.108.024003](https://doi.org/10.1103/PhysRevC.108.024003)

## I. INTRODUCTION

In this paper we present the results of the extended-soft-core (ESC) model ESC16 for channels with total strangeness  $S = -3$  and  $-4$ . This is a further  $SU(3)$  generalization of the ESC16 models on  $NN$  [1],  $YN$  [2], and  $YY$  [3] for baryon-baryon channels, which are henceforth referred to as paper I, paper II, and paper III, respectively. A similar approach has been performed in Ref. [4], where the Nijmegen soft-core one-boson-exchange (OBE) interactions NSC97a-f for baryon-baryon ( $BB$ ) systems for  $S = -2$ ,  $-3$ , and  $-4$  were presented.

This paper forms the completion of the study of baryon-baryon interactions with the ESC interactions, comprising all  $\{8\} \otimes \{8\}$  channels, i.e., all strangeness  $S = 0$ ,  $-1$ ,  $-2$ ,  $-3$ , and  $-4$  channels. The basis of this work is broken  $SU(3)$  symmetry and the  $NN$ ,  $YN$ , and  $YY$  data. In this paper we show the  $S = -3$  and  $-4$  results for the ESC16 model, which can be considered being typical for this approach to the  $BB$  interactions. (For results and review of former versions ESC04 and ESC08 as well as applications to hypernuclei for  $S = 0$ ,  $-1$ , and  $-2$ , see Ref. [5].)

The OBE model NSC97 [4] and the ESC models are the first models for which the  $S < -2$  interactions contain no free parameters. Compared to NSC97 the overall description of the  $BB$  interaction in the ESC models is clearly

an improvement. In the ESC models the  $S = 0$ ,  $-1$ , and  $-2$  interactions are fitted very successfully to the two-body scattering data. For  $S = -2$  there is a difficulty with (i) the  $\Xi^-p$  correlations found in the ALICE experiment at CERN [6–8] and (ii) the J-PARC/E05 data on  $^{12}_{\Xi}\text{Be}$  [9]. This hints at an incompleteness of the  $BB$  interactions in ESC04, ESC08, and ESC16. To account for this in the ESC16\*(A, B) versions,  $SU(3)$ -symmetric contact terms have been added.

After the Nijmegen work [4], all  $BB$  channels have been studied also in the framework of the resonating-group method (RGM) using the  $SU(6)$  quark model [10]. Furthermore in the past years there have also been studies of the  $S = -3$  and  $-4$  systems using  $BB$  interactions from lattice QCD (LQCD) [11,12], and recently also results for  $S = -3$  and  $-4$  have been given from  $BB$  interactions from chiral-effective-field theory [13].

For the  $S = -3$  and  $-4$  channels virtually no experimental scattering information is available, except preliminary  $\Xi^-\Xi^-$  and  $\Xi^-\Lambda$  correlation data [14]. Also the information from hypernuclei is nonexistent. For  $S = -2$  there are data on  $\Lambda\Lambda$  hypernuclei, which became very much improved by the observation of the Nagara event [15]. This event indicates that the  $\Lambda\Lambda$  interaction is rather weak, in contrast to the estimates based on the older experimental observations [16,17]. This has always been a characteristic feature of the Nijmegen soft-core models. The ESC16 model describes all experimental information on the  $S = 0$ ,  $-1$ , and  $-2$  systems, two-body scattering, and hypernuclei very satisfactorily. An exception

\*[t.rijken@science.ru.nl](mailto:t.rijken@science.ru.nl)

is the (weakly) repulsive  $\Xi$ -nucleus interaction, which is attractive experimentally. This is repaired with ESC16\*(A, B).

Recently more  $\Xi$  hypernuclei have been studied and observed [18–20], also indicating that the  $\Xi$ -nucleus interaction is attractive and the  $\Xi N$ - $\Lambda\Lambda$  coupling is weak [21].

Also, the ESC models are rather in accordance with QCD (see Refs. [1–3,22,23] for an exposition of the arguments). Therefore, the predictions for the  $S = -3$  and  $-4$  channels can be expected to be realistic.

The study of strangeness-rich systems in astrophysics is an important topic in the past 60 years with many contributions. We refer to the (general) review papers [24,25] for references. In particular, the  $\Lambda$ -hyperon puzzle in neutron star matter [26] is reviewed in Ref. [25]. Strangeness-rich systems can be exotic multiquark systems consisting of up ( $u$ ), down ( $d$ ), and strange ( $s$ ) quarks, like the elusive  $H$  dibaryon, a six-quark  $uuddss$  system predicted by Jaffe [27]. But they can also simply be bound states of nucleons ( $N$ ), hyperons ( $Y = \Lambda$  and  $\Sigma$ ), and cascades ( $\Xi$ ). To get a better handle on the latter possibility, we are in need of potential models that describe all possible interactions between nucleons, hyperons, and cascades.

In the virtual absence of experimental information for  $S = -3$  and  $-4$ , we assume that the potentials obey (broken) flavor SU(3) symmetry. As in papers I–III, the  $S = -3$  and  $-4$  potentials are parametrized in terms of meson-baryon-baryon and meson-pair-baryon-baryon couplings and Gaussian form factors. This enables us to include in the interaction one-boson exchange (OBE), two-pseudoscalar exchange (TME), and meson-pair exchange (MPE), without any new parameters. All parameters have been fixed by a simultaneous fit to the  $NN$  and  $YN$  data, scattering and hypernuclear, see papers I and II. Each  $NN \oplus YN$  model leads to a  $YY$  model in a well-defined way. SU(3) symmetry allows us to define all coupling constants needed to describe the multistrange interactions in the baryon-baryon channels occurring in  $\{8\} \otimes \{8\}$ . In all ESC models it is assumed that the coupling constants, apart from meson mixing, are SU(3) symmetric. The success of the ESC models suggests that for the coupling constants deviations from SU(3) symmetry are small.

In paper III, new phenomenological Gaussian SU(3)-symmetric two-body  $BB$  potentials are introduced in addition to the meson and meson-pair exchanges to investigate the possible incompleteness of the ESC interactions considered thus far in the ESC models. The motivation for this are the recent  $S = -2$  hypernuclei experimental observations [9,28,29] and  $G$ -matrix calculations [30]. Also, ESC16 fails to describe the  $\Xi^-p$  correlations found in the ALICE experiment at CERN [6,8]. Then, fitting to the  $NN \oplus YN \oplus YY$  data resulted in good  $BB$  well depths. In this paper we include the  $S = -3$  and  $-4$  results for ESC16 and the effective range parameters for the two variants ESC16\*(A) and ESC16\*(B) [3].

Most of the details on the SU(3) description are well known, and, in particular, for baryon-baryon scattering they can be found in papers I–III and, e.g., Refs. [31,32]. So, here we restrict ourselves to a minimal exposition of these matters, necessary for the readability of this paper.

The contents of this paper are as follows. In Sec. II the  $S = -3$  and  $-4$  thresholds are displayed and the multichannel description is reviewed. Furthermore, for completeness we repeat the SU(3)-symmetric interaction Lagrangian describing the interaction vertices between mesons and members of the  $J^P = (1/2)^+$  baryon octet, and we define their coupling constants. We then identify the various channels that occur in the  $S = -3$  and  $-4$  baryon-baryon systems. We describe the R-conjugation operation, which is useful for the comparison of the  $(\Lambda\Xi, \Sigma\Xi)$  and  $(\Lambda N, \Sigma N)$  potentials. In Sec. III the numerical values of the used baryon masses and of the thresholds' momenta are listed. In Sec. IV the meson- and meson-pair baryon-baryon couplings are addressed. In Sec. V the results for the multichannel effective-range parameters, partial-wave phase shifts, and inelasticity parameters are given, and possible bound states are considered. In Sec. VI the paper is concluded with a short discussion and summary.

In Appendix A the SU(3) irreps and baryon-baryon isospin states are displayed. In Appendix B, tables with the OBE meson coupling constants are given, and in Appendix C the meson-pair coupling MPEs for the models ESC16 and ESC16\*(A, B) are given. In Appendix D tables with the coupled-channel phase parameters are shown for model ESC16.

## II. CHANNELS, POTENTIALS, AND SU(3) SYMMETRY

### A. Multichannel formalism

For the kinematics and the definition of the amplitudes, we refer to paper II of this series. Similar material can be found in Ref. [32]. Also, in paper I the derivation of the Lippmann-Schwinger equation in the context of the relativistic two-body equation is described.

On the physical particle basis, there are four charge channels:

$$\begin{aligned} q = +1: & \quad \Sigma^+ \Xi^0 \rightarrow \Sigma^+ \Xi^0, \\ q = 0: & \quad (\Lambda \Xi^0, \Sigma^0 \Xi^0, \Sigma^+ \Xi^-) \\ & \quad \rightarrow (\Lambda \Xi^0, \Sigma^0 \Xi^0, \Sigma^+ \Xi^-); \Xi^0 \Xi^0 \rightarrow \Xi^0 \Xi^0, \\ q = -1: & \quad (\Lambda \Xi^-, \Sigma^0 \Xi^-, \Sigma^- \Xi^0) \\ & \quad \rightarrow (\Lambda \Xi^-, \Sigma^0 \Xi^-, \Sigma^- \Xi^0); \Xi^0 \Xi^- \rightarrow \Xi^0 \Xi^-, \\ q = -2: & \quad \Sigma^- \Xi^- \rightarrow \Sigma^- \Xi^-; \Xi^- \Xi^- \rightarrow \Xi^- \Xi^-. \end{aligned} \quad (2.1)$$

We note here that in strong interactions  $S$  is conserved and hence in the  $q = -1$  and  $-2$  channels there is no coupling of the  $\Xi\Xi$  channels in Eq. (2.1) with the others.

Like in Refs. [31,32] and in papers I–III, the potentials are calculated on the isospin basis. For  $S = -3$  and  $-4$  hyperon-hyperon systems there are three isospin channels:

$$\begin{aligned} Y = -1, S = -3, I = 1/2: & \quad (\Lambda\Xi, \Sigma\Xi \rightarrow \Lambda\Xi, \Sigma\Xi), \\ Y = -1, S = -3, I = 3/2: & \quad (\Sigma\Xi \rightarrow \Sigma\Xi), \\ Y = -2, S = -4, I = 0, 1: & \quad (\Xi\Xi \rightarrow \Xi\Xi). \end{aligned} \quad (2.2)$$

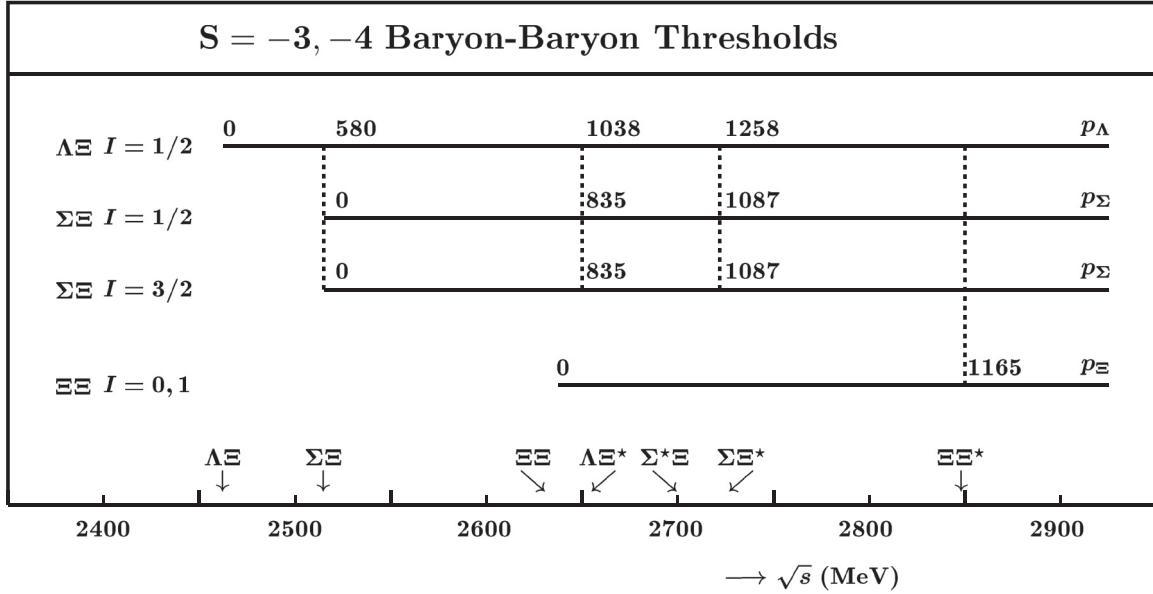


FIG. 1. Thresholds in  $YY$  channels for  $S = -3$  and  $-4$ . The laboratory momenta  $p_\Lambda$ ,  $p_\Sigma$ , and  $p_\Xi$  are given in  $\text{MeV}/c^2$ .

The relation between the charge ( $Q$ ), isospin ( $I$ ), and hypercharge ( $Y$ ) is given by the Gell-Mann-Nishijima relation  $Q = Y/2 + I_3$ , where in terms of the baryon number ( $B$ ) and strangeness ( $S$ ) the hypercharge  $Y = B + S$ .

The two-particle thresholds in the  $YY$  channels for  $S = -3$  and  $-4$  are shown in Fig. 1. For  $\Lambda\Xi$  at the  $\Sigma\Xi$  and  $\Lambda\Xi^*$  thresholds, the (average)  $p_\Lambda$  laboratory momenta are indicated. Similarly for  $\Sigma\Xi$ , the  $p_\Sigma$  at the  $\Sigma\Xi^*$  threshold are indicated. For the  $\Xi\Xi$  at the  $\Xi\Xi^*$  threshold, the  $p_\Xi$  is shown. Here, only the  $J^P = 1/2^+$  octet and  $J^P = 3/2^+$  decuplet baryons are considered.

For the kinematics of the reactions and the various thresholds, see Ref. [31]. In this work we do not solve the Lippmann-Schwinger equation, but rather the multichannel Schrödinger equation in configuration space, completely analogous to Ref. [32]. The multichannel Schrödinger equation for the configuration-space potential is derived from the Lippmann-Schwinger equation through the standard Fourier transform, and the equation for the radial wave function is

found to be of the form [32]

$$u''_{l,j} + (p_l^2 \delta_{i,j} - A_{i,j})u_{l,j} - B_{i,j}u'_{l,j} = 0, \quad (2.3)$$

where  $A_{i,j}$  contains the potential, nonlocal contributions and the centrifugal barrier, while  $B_{i,j}$  is only present when nonlocal contributions are included. The solution in the presence of open and closed channels is given, for example, in Ref. [33]. The inclusion of the Coulomb interaction in the configuration-space equation is well known and included in the evaluation of the scattering matrix. The Coulomb interaction is present only in the channels  $\Sigma^+\Xi^-$  and  $\Xi^-\Xi^-$ .

Obviously, the potentials on the particle basis for the  $Y = -2$  channels are given by the  $I = 0$  and  $I = 1$   $\Xi\Xi$  potentials on the isospin basis. For  $Y = -1$  channels the potentials are related to the potentials on the isospin basis by an isospin rotation. Ordering the channels in the  $q = 0$  sector according to increasing rest mass ( $\Lambda\Xi^0$ ,  $\Sigma^0\Xi^0$ ,  $\Sigma^+\Xi^-$ ), one obtains in channel space the potential matrix  $V_{ab}(I) \equiv V_{a,\Xi;b,\Xi}(I)$ , with  $a, b \equiv \Lambda, \Sigma$ ,

$$V(q = 0, Y = -1) = \begin{pmatrix} V_{\Lambda\Lambda}(\frac{1}{2}) & -\sqrt{\frac{1}{3}}V_{\Lambda\Sigma} & \sqrt{\frac{2}{3}}V_{\Lambda\Sigma} \\ -\sqrt{\frac{1}{3}}V_{\Lambda\Sigma} & \frac{1}{3}[V_{\Sigma\Sigma}(\frac{1}{2}) + 2V_{\Sigma\Sigma}(\frac{3}{2})] & \frac{\sqrt{2}}{3}[-V_{\Sigma\Sigma}(\frac{1}{2}) + V_{\Sigma\Sigma}(\frac{3}{2})] \\ \sqrt{\frac{2}{3}}V_{\Lambda\Sigma} & \frac{\sqrt{2}}{3}[-V_{\Sigma\Sigma}(\frac{1}{2}) + V_{\Sigma\Sigma}(\frac{3}{2})] & \frac{1}{3}[2V_{\Sigma\Sigma}(\frac{1}{2}) + V_{\Sigma\Sigma}(\frac{3}{2})] \end{pmatrix}, \quad (2.4)$$

and for  $q = -1$  we have now the ordering ( $\Lambda\Xi^-$ ,  $\Sigma^-\Xi^0$ ,  $\Sigma^0\Xi^-$ ), and we get the following for the potential matrix:

$$V(q = -1, Y = -1) = \begin{pmatrix} V_{\Lambda\Lambda}(\frac{1}{2}) & -\sqrt{\frac{2}{3}}V_{\Lambda\Sigma} & \sqrt{\frac{1}{3}}V_{\Lambda\Sigma} \\ -\sqrt{\frac{2}{3}}V_{\Lambda\Sigma} & \frac{1}{3}[2V_{\Sigma\Sigma}(\frac{1}{2}) + V_{\Sigma\Sigma}(\frac{3}{2})] & \frac{\sqrt{2}}{3}[-V_{\Sigma\Sigma}(\frac{1}{2}) + V_{\Sigma\Sigma}(\frac{3}{2})] \\ \sqrt{\frac{1}{3}}V_{\Lambda\Sigma} & \frac{\sqrt{2}}{3}[-V_{\Sigma\Sigma}(\frac{1}{2}) + V_{\Sigma\Sigma}(\frac{3}{2})] & \frac{1}{3}[V_{\Sigma\Sigma}(\frac{1}{2}) + 2V_{\Sigma\Sigma}(\frac{3}{2})] \end{pmatrix}. \quad (2.5)$$

TABLE I. SU(3) content of the different interaction channels.  $S$  is the total strangeness and  $I$  is the isospin. The upper half refers to the space-spin symmetric states  $^3S_1, ^1P_1, ^3D_1, \dots$ , while the lower half refers to the space-spin antisymmetric states  $^1S_0, ^3P_1, ^1D_2, \dots$

Space-spin symmetric states			
$S$	$I$	Channels	SU(3) irreps
0	0	$NN$	$\{10^*\}$
-1	1/2	$\Lambda N, \Sigma N$	$\{10^*\}, \{8\}_a$
	3/2	$\Sigma N$	$\{10\}$
-2	0	$\Xi N$	$\{8\}_a$
	1	$\Xi N, \Sigma \Sigma$	$\{10\}, \{10^*\}, \{8\}_a$
		$\Sigma \Lambda$	$\{10\}, \{10^*\}$
-3	1/2	$\Xi \Lambda, \Xi \Sigma$	$\{10\}, \{8\}_a$
	3/2	$\Xi \Sigma$	$\{10^*\}$
-4	0	$\Xi \Xi$	$\{10\}$
Space-spin antisymmetric states			
$S$	$I$	Channels	SU(3) irreps
0	1	$NN$	$\{27\}$
-1	1/2	$\Lambda N, \Sigma N$	$\{27\}, \{8\}_s$
	3/2	$\Sigma N$	$\{27\}$
-2	0	$\Lambda \Lambda, \Xi N, \Sigma \Sigma$	$\{27\}, \{8\}_s, \{1\}$
	1	$\Xi N, \Sigma \Lambda$	$\{27\}, \{8\}_s$
	2	$\Sigma \Sigma$	$\{27\}$
-3	1/2	$\Xi \Lambda, \Xi \Sigma$	$\{27\}, \{8\}_s$
	3/2	$\Xi \Sigma$	$\{27\}$
-4	1	$\Xi \Xi$	$\{27\}$

The connection between the  $BB$  isospin states and the SU(3) irreps is given in Table I, and in the figures of Appendix A, the  $NN$ ,  $YN$ , and  $YY$  data are given for the irreps  $\{8\}$ ,  $\{27\}$ ,  $\{10^*\}$ ,  $\{10\}$ , and  $\{1\}$ .

The momentum space and configuration space potentials for the ESC16 model have been described in papers I and II for baryon-baryon in general. Therefore, they apply also to hyperon-hyperon and we can refer for that part of the potential to these papers. Also in the ESC model, the potentials are of such a form that they are exactly equivalent in both momentum space and configuration space. The treatment of the mass differences among the baryons is handled exactly as is done in Refs. [31,32]. Also, exchange potentials related to the strange-meson exchange  $K, K^*$ , etc., can be found in these references.

The baryon mass differences in the intermediate states for TME and MPE potentials have been neglected for  $YN$  and  $YY$  scattering. This, although possible in principle, becomes rather laborious and is not expected to change the characteristics of the baryon-baryon potentials.

### B. SU(3) Symmetry and R conjugation

The SU(3)-invariant interaction Hamiltonian for the baryon-baryon ( $BB$ ) pseudoscalar ( $P$ ) meson interaction reads [34]

$$\mathcal{H}_I = g_{P,8} \sqrt{2} [\alpha_P [\bar{B}BP]_F + (1 - \alpha_P) [\bar{B}BP]_D] + g_{P,1} [\bar{B}BP]_S. \quad (2.6)$$

TABLE II. SU(3) contents of the various potentials on the isospin basis.

Space-spin antisymmetric states $^1S_0, ^3P_1, ^1D_2, \dots$			
$\Xi \Xi \rightarrow \Xi \Xi$	$Y = -2, I = 1$	$V_{\Xi \Xi} (I = 1) = V_{27}$	
$\Lambda \Xi \rightarrow \Lambda \Xi$		$V_{\Lambda \Lambda} (I = \frac{1}{2}) = (9V_{27} + V_{8_s})/10$	
$\Lambda \Xi \rightarrow \Sigma \Xi$	$Y = -1, I = \frac{1}{2}$	$V_{\Sigma \Lambda} (I = \frac{1}{2}) = (-3V_{27} + 3V_{8_s})/10$	
$\Sigma \Xi \rightarrow \Sigma \Xi$		$V_{\Sigma \Sigma} (I = \frac{1}{2}) = (V_{27} + 9V_{8_s})/10$	
$\Sigma \Xi \rightarrow \Sigma \Xi$	$Y = -1, I = \frac{3}{2}$	$V_{\Sigma \Sigma} (I = \frac{3}{2}) = V_{27}$	
Space-spin symmetric states $^3S_1, ^1P_1, ^3D_1, \dots$			
$\Xi \Xi \rightarrow \Xi \Xi$	$Y = -2, I = 0$	$V_{\Xi \Xi} (I = 0) = V_{10}$	
$\Lambda \Xi \rightarrow \Lambda \Xi$		$V_{\Lambda \Lambda} (I = \frac{1}{2}) = (V_{10} + V_{8_a})/2$	
$\Lambda \Xi \rightarrow \Sigma \Xi$	$Y = -1, I = \frac{1}{2}$	$V_{\Sigma \Lambda} (I = \frac{1}{2}) = (V_{10} - V_{8_a})/2$	
$\Sigma \Xi \rightarrow \Sigma \Xi$		$V_{\Sigma \Sigma} (I = \frac{1}{2}) = (V_{10} + V_{8_a})/2$	
$\Sigma \Xi \rightarrow \Sigma \Xi$	$Y = -1, I = \frac{3}{2}$	$V_{\Sigma \Sigma} (I = \frac{3}{2}) = V_{10^*}$	

Here, the baryons are the members of the  $J^P = \frac{1}{2}^+$  baryon octet

$$B = \begin{pmatrix} \frac{\Sigma^0}{\sqrt{2}} + \frac{\Lambda}{\sqrt{6}} & \Sigma^+ & p \\ \Sigma^- & -\frac{\Sigma^0}{\sqrt{2}} + \frac{\Lambda}{\sqrt{6}} & n \\ -\Xi^- & \Xi^0 & -\frac{2\Lambda}{\sqrt{6}} \end{pmatrix}. \quad (2.7)$$

The meson nonet  $3 \times 3$  matrix  $P$  can be written as

$$P = P_{\{1\}} + P_{\{8\}}, \quad (2.8)$$

where the singlet  $3 \times 3$  matrix  $P_{\{1\}}$  has the elements  $\eta_0/\sqrt{3}\delta_{\beta}^{\alpha}$ , and the octet matrix  $P_{\{8\}}$  is given by

$$P_{\{8\}} = \begin{pmatrix} \frac{\pi^0}{\sqrt{2}} + \frac{\eta_8}{\sqrt{6}} & \pi^+ & K^+ \\ \pi^- & -\frac{\pi^0}{\sqrt{2}} + \frac{\eta_8}{\sqrt{6}} & K^0 \\ K^- & \bar{K}^0 & -\frac{2\eta_8}{\sqrt{6}} \end{pmatrix}. \quad (2.9)$$

Similarly, the interaction with the vector  $J^{\text{PC}} = 1^{--}$ , with scalar  $J^{\text{PC}} = 0^{++}$ , and with axial vectors  $J^{\text{PC}} = 1^{++}$  and  $J^{\text{PC}} = 1^{+-}$  mesons. With the SU(2) isosinglet  $\Lambda$ , isodoublets

$$N = \begin{pmatrix} p \\ n \end{pmatrix}, \quad \Xi = \begin{pmatrix} \Xi^0 \\ \Xi^- \end{pmatrix}, \quad \text{and} \quad K = \begin{pmatrix} K^+ \\ K^0 \end{pmatrix}, \quad K_c = \begin{pmatrix} \bar{K}^0 \\ -K^- \end{pmatrix}, \quad (2.10)$$

and isovectors  $(\Sigma^+, \Sigma^0, \Sigma^-)$  and  $(\pi^+, \pi^0, \pi^-)$ , the SU(3)-invariant interaction Hamiltonian (2.6) can be written in the isospin basis (see, e.g., Refs. [3,34]), formula (2.9). All coupling constants can be expressed in terms of only four parameters. The explicit expressions can be found in Refs. [31,34]. For example, in the case of the pseudoscalar mesons the parameters are (i) the octet coupling  $g_{NN\pi}$ , the  $F/(F+D)$  ratio  $\alpha_P$ , the singlet coupling  $g_{\eta_0}$ , and the  $\eta_8 - \eta_0$  mixing angle  $\theta_P$ . In Table II, the relation between the potentials on the isospin basis is given [see Eqs. (2.4) and (2.5) and the SU(3) irreps]. Here  $V_{\Xi \Xi} = V_{\Xi \Xi, \Xi \Xi}$ ,  $V_{\Lambda \Lambda} = V_{\Lambda \Xi, \Lambda \Xi}$ , etc.

In paper III we have introduced as an extension of the ESC16 model, the ESC16\* models A and B with additional

TABLE III. ESC16\*(A): Coupling constants' SU(3)-symmetric Gaussian potentials.

$\{\mu\}$	$\{27\}$	$\{8_s\}$	$\{1\}$	$\{8_a\}$	$\{10^*\}$	$\{10\}$
$A_{\{\mu\}}$	-0.109	-0.219	-1.568	-3.322	-0.635	-0.635
$B_{\{\mu\}}$	0.156	-0.356	0.459	3.594	0.123	0.123

SU(3)-symmetric central and spin-spin Gaussian-contact  $BB$   $s$ -channel potentials

$$W_{\mu,c}(r) = A_{\mu}f_W(r), \quad W_{\mu,\sigma}(r) = B_{\mu}f_W(r)\sigma_1 \cdot \sigma_2,$$

where  $f_W(r) = m_W \exp(-m_W^2 r^2)$ ,  $m_W = 300$  MeV. The  $s$ -channel coefficients  $A_{\mu}$  and  $B_{\mu}$  for ESC16\*(A) are derived from Tables XVIII and XIX in paper III and are given in Table III. Here, we have chosen to exhibit the  $s$ -channel contact potentials rather than the  $t$ - and  $u$ -channel ones in paper III. The largest contact potentials occur in the  $\{8_a\}$  and  $\{1\}$  irreps. The  $s$ -channel coefficients for model ESC16\*(B) with R symmetry [35] for the Gaussian contact  $BB$  potentials are given in Table IV.

For model ESC16\*(A) the entries for the irreps  $\{10\}$  and  $\{10^*\}$  in Table III are the same. The reason is that we neglect the  $\{8_s\} \leftrightarrow \{8_a\}$  transitions in the contact potentials. These lead to spin singlet-triplet transitions  $^1P_1 \leftrightarrow ^3P_1$ , etc., which are small and do not occur in  $s$  waves. So, *de facto* the contact potentials have R symmetry.

To compare the SU(3) structure for the  $BB$  states, Gell-Mann's R conjugation [35,36] is useful. R conjugation is the inversion operation on the baryon and pseudoscalar octet states

$$p \leftrightarrow \Xi^-, \quad n \leftrightarrow \Xi^0, \quad \Lambda \leftrightarrow \Lambda, \quad \Sigma^0 \leftrightarrow \Sigma^0, \quad (2.11)$$

$$K^+ \leftrightarrow K^-, \quad K^0 \leftrightarrow \bar{K}^0, \quad \eta \leftrightarrow \eta, \quad \pi^0 \leftrightarrow \pi^0. \quad (2.12)$$

For the  $BB$  states one has

$$\begin{aligned} R\psi_{27}(Y, I, I_3) &= \psi_{27}(-Y, I, -I_3), \\ R\psi_{10}(Y, I, I_3) &= \psi_{10^*}(-Y, I, -I_3), \\ R\psi_{8_s}(Y, I, I_3) &= \psi_{8_s}(-Y, I, -I_3), \\ R\psi_{8_a}(Y, I, I_3) &= -\psi_{8_a}(-Y, I, -I_3), \\ R\psi_1(Y, I, I_3) &= \psi_1(-Y, I, -I_3). \end{aligned} \quad (2.13)$$

Therefore, in comparing the SU(3) structure of the  $(\Lambda N, \Sigma N)$  potentials with the  $(\Lambda \Xi, \Sigma \Xi)$  potentials, the irreps  $\{10\}$  and  $\{10^*\}$  are interchanged, and similarly for the  $NN$  potentials and the  $\Xi \Xi$  potentials. The entries of Table II, apart from using SU(3) Clebsch-Gordan coefficients, can be derived from Table I in Ref. [2] using R conjugation.

TABLE IV. ESC16\*(B): Coupling constants' SU(3)-symmetric Gaussian potentials.

$\{\mu\}$	$\{27\}$	$\{8_s\}$	$\{1\}$	$\{8_a\}$	$\{10^*\}$	$\{10\}$
$A_{\{\mu\}}$	-0.118	0.071	-0.874	-3.003	-1.635	-1.635
$B_{\{\mu\}}$	0.261	-0.851	0.084	3.268	-0.302	-0.302

TABLE V. Isospin factors for the various meson exchanges in the different channels with total strangeness and isospin.  $P_f$  is the flavor-exchange operator. Nonexisting channels are marked by a long dash.

$S = -3$	$I = 1/2$	$I = 3/2$
$(\Lambda \Xi   \eta, \eta'   \Lambda \Xi)$	1	—
$(\Sigma \Xi   \eta, \eta'   \Sigma \Xi)$	1	1
$(\Sigma \Xi   \pi   \Sigma \Xi)$	-2	1
$(\Sigma \Xi   \pi   \Lambda \Xi)$	$\sqrt{3}$	—
$(\Lambda \Xi   K   \Xi \Lambda)$	$P_f$	—
$(\Sigma \Xi   K   \Sigma \Xi)$	$-P_f$	$2P_f$
$(\Lambda \Xi   K   \Xi \Sigma)$	$P_f \sqrt{3}$	—
$S = -4$	$I = 0$	$I = 1$
$(\Xi \Xi   \eta, \eta'   \Xi \Xi)$	$\frac{1}{2}(1 - P_f)$	$\frac{1}{2}(1 + P_f)$
$(\Xi \Xi   \pi   \Xi \Xi)$	$-\frac{3}{2}(1 - P_f)$	$\frac{1}{2}(1 + P_f)$

The R conjugation is not an SU(3) transformation, and also it is not a symmetry of the strong interactions. The latter would mean no  $\{8_s\} \leftrightarrow \{8_a\}$  transitions, because  $\langle \{8_a\} | V | \{8_s\} \rangle = \langle \{8_a\} | R^{-1} V R | \{8_s\} \rangle = -\langle \{8_a\} | V | \{8_s\} \rangle = 0$ . This would imply that the transitions  $^1P_1 \leftrightarrow ^3P_1$  are forbidden, and so there would be no antisymmetric spin-orbit forces. However, for the vector exchange and the axial-vector exchange with different  $F/(F+D)$  ratios for the direct and derivative couplings the antisymmetric spin-orbit potentials are nonzero, while having SU(3) symmetry. The extra restriction from R-conjugation symmetry with respect to SU(3) is that  $V_{\{10\}} = V_{\{10^*\}}$ . Then, the central, spin-spin, tensor, spin-orbit, and quadratic spin-orbit potentials have R symmetry for exact SU(3) symmetry. In the ESC models,  $V_{10} \approx V_{10^*}$  (see Ref. [3]), and the singlet-triplet transitions are small. So, we conclude that R conjugation is an approximate symmetry in the ESC models and is broken “kinematically,” similar to SU(3).

### C. Solving the multichannel Schrödinger equation

The method of evaluation of the ESC16 models for the  $S = -3$  and  $-4$  channels follows closely that for the  $S = 0, -1$ , and  $-2$  channels. For details, see paper III [3], Secs. II and III. The main features are the following.

- (i) The multichannel Schrödinger equation is solved for the physical particle channels. The  $S = -3$  and  $-4$   $BB$  channels can be classified according to their total charge  $Q$ ; these are given in Eq. (2.1).
- (ii) Average baryon and meson masses are used in the potentials; i.e., isospin is treated as a good quantum number. The only breaking of isospin symmetry occurs via the inclusion of the Coulomb interaction.
- (iii) The isospin matrix elements for the various OBE potentials are given in Table V, where we use the pseudoscalar mesons as a specific example. The flavor-exchange operator  $P_f$  is +1 for a flavor symmetric state and -1 for a flavor antisymmetric state. Since two-baryon states are totally antisymmetric,



TABLE VI. Baryon masses in MeV/ $c^2$ .

Baryon		Mass
Nucleon	$p$	938.2796
	$n$	939.5731
Hyperon	$\Lambda$	1115.60
	$\Sigma^+$	1189.37
	$\Sigma^0$	1192.46
	$\Sigma^-$	1197.436
Cascade	$\Xi^0$	1314.90
	$\Xi^-$	1321.32

$P_f = -P_x P_\sigma$ . Therefore, the exchange operator  $P_f$  has the value  $P_f = +1$  for even- $L$  singlet and odd- $L$  triplet partial waves and  $P_f = -1$  for odd- $L$  singlet and even- $L$  triplet partial waves. For total strangeness  $S = -3$ , the final-state interchanged diagram only occurs when the exchanged meson carries strangeness ( $K, K^*, \kappa, K^{**}$ ).

- (iv) For a proper derivation of the exchange operator  $P_f$  and the exchange forces, see Ref. [3], Sec. III.

### III. MULTICHANNEL THRESHOLDS $S = -3$ CHANNELS

As seen from Eq. (2.1) the  $S = -3$  two-baryon channels consist of two separate coupled-channel systems separated by the charge. The thresholds are due to the baryon mass differences. The used baryon masses are the same as those in Refs. [1–3] and are given in Table VI. The laboratory momenta, starting from the baryons at the lowest threshold, are shown in Fig. 1. Taking the charge dependence of the masses into account gives a splitting of the thresholds, e.g.,

for  $(\Lambda \Xi^-, \Sigma^- \Xi^0, \Sigma^0 \Xi^-)$ ,

$$\begin{aligned} p_\Lambda^{\text{th}}(\Lambda \Xi^- \rightarrow \Sigma^- \Xi^0) &= 578.9 \text{ MeV}/c, \\ p_\Lambda^{\text{th}}(\Lambda \Xi^- \rightarrow \Sigma^0 \Xi^-) &= 584.8 \text{ MeV}/c, \end{aligned} \quad (3.1)$$

for  $(\Lambda \Xi^0, \Sigma^0 \Xi^0, \Sigma^+ \Xi^-)$ ,

$$\begin{aligned} p_\Lambda^{\text{th}}(\Lambda \Xi^0 \rightarrow \Sigma^0 \Xi^0) &= 572.2 \text{ MeV}/c, \\ p_\Lambda^{\text{th}}(\Lambda \Xi^0 \rightarrow \Sigma^+ \Xi^-) &= 585.5 \text{ MeV}/c. \end{aligned} \quad (3.2)$$

The meson masses are the same as those in Refs. [1–3], as well as the cutoff masses. The threshold differences lead to effective masses for the meson with nonzero strangeness (see Refs. [3,4,37] for details and references). For  $S = -3$  channels these masses are for the pseudoscalar meson  $m_K = 453.4$  MeV and the vector meson  $m_{K^*} = 869.1$  MeV. These effects are not included for the scalar and axial mesons.

A further subdivision is according to the total isospin. The different thresholds have been discussed in detail in Ref. [4], and we show them here in Fig. 1 for the purpose of general orientation. Their presence turns the Lippmann-Schwinger and Schrödinger equations into a coupled-channel matrix equation, where the different channels open up at different energies. In general one has a combination of “open” and “closed” channels. For a discussion of the solution of such a mixed system, we refer the reader to Ref. [37].

### IV. ESC MODEL PARAMETERS

Complete sets of meson coupling constants for ESC16 and ESC16\* are given in Appendix B, Tables VII, and VIII, respectively. The corresponding meson-pair couplings are given in Appendix C, Tables IX, and X, respectively. For other model parameters, such as Gaussian cutoff’s, meson mixing angles, etc., see Refs. [1–3].

### V. RESULTS

The main purpose of this paper is to present the properties of the ESC16 and ESC16\* potentials for the  $S = -3$  and  $-4$  sectors. We found that the results for  $S = -3$  and  $-4$  for the different models are not significantly different. We show the detailed results for ESC16, which are sufficient to represent the possible kinds of results.

In the following we present the model predictions for scattering lengths, bound states, and cross sections.

#### A. Effective-range parameters

The (multichannel) effective-range expansion (see Ref. [33]) reads

$$p^{L+1/2}(\bar{K}^J)^{-1} p^{L+1/2} - A^{-1} + \frac{1}{2}(p^2 - p_0^2)^{1/2} R (p^2 - p_0^2)^{1/2},$$

where  $\bar{K}^J$  is the mutilated  $K^J$  matrix with the  $^3D_1$  channels being cut out,  $A^{-1}$  is the inverse scattering-length matrix,  $R$  is the effective-range matrix, and  $p^{L+1/2}$  and  $(p^2 - p_0^2)^{1/2}$  are the diagonal matrices with elements  $p_i^{L+1/2}$  and  $(p_i^2 - p_{0i}^2)^{1/2}$ . Here,  $p_{0i}$  denotes the momentum at the  $\Sigma \Xi^0$  threshold (see below).

Next, we give the low-energy parameters, i.e., scattering lengths and effective ranges, for the following models.

#### B. $S = -4$ results

The following  $S = -4$  low-energy parameters of ESC16 were obtained, where the C denotes Coulomb included:

$$\begin{aligned} a_{\Xi\Xi}^C(^1S_0) &= -1.81 \text{ fm}, \quad r_{\Xi\Xi}^C(^1S_0) = 3.89 \text{ fm}, \\ a_{\Xi\Xi}(^1S_0) &= -1.90 \text{ fm}, \quad r_{\Xi\Xi}(^1S_0) = 4.28 \text{ fm}, \\ a_{\Xi\Xi}(^3S_1) &= +0.52 \text{ fm}, \quad r_{\Xi\Xi}(^3S_1) = 2.74 \text{ fm}. \end{aligned}$$

For ESC16\*(A), we obtained

$$\begin{aligned} a_{\Xi\Xi}(^1S_0) &= -1.69 \text{ fm}, \quad r_{\Xi\Xi}(^1S_0) = 4.71 \text{ fm}, \\ a_{\Xi\Xi}(^3S_1) &= +0.48 \text{ fm}, \quad r_{\Xi\Xi}(^3S_1) = 3.41 \text{ fm}. \end{aligned}$$

For ESC16\*(B), we obtained

$$\begin{aligned} a_{\Xi\Xi}(^1S_0) &= -1.86 \text{ fm}, \quad r_{\Xi\Xi}(^1S_0) = 4.45 \text{ fm}, \\ a_{\Xi\Xi}(^3S_1) &= +0.49 \text{ fm}, \quad r_{\Xi\Xi}(^3S_1) = 3.16 \text{ fm}. \end{aligned}$$

#### C. $S = -3$ and $I = 3/2$ results

For ESC16, we obtained

$$\begin{aligned} a_{\Sigma\Xi^0}(^1S_0) &= -1.71 \text{ fm}, \quad r_{\Sigma\Xi^0}(^1S_0) = 3.71 \text{ fm}, \\ a_{\Sigma\Xi^0}(^3S_1) &= -0.85 \text{ fm}, \quad r_{\Sigma\Xi^0}(^3S_1) = 8.02 \text{ fm}. \end{aligned}$$

For ESC16\*(A), we obtained

$$a_{\Sigma\Xi}(^1S_0) = -1.41 \text{ fm}, \quad r_{\Sigma\Xi}(^1S_0) = 4.29 \text{ fm},$$

$$a_{\Sigma\Xi}(^3S_1) = -1.31 \text{ fm}, \quad r_{\Sigma\Xi}(^3S_1) = 5.47 \text{ fm}.$$

For ESC16\*(B), we obtained

$$a_{\Sigma\Xi}(^1S_0) = -1.64 \text{ fm}, \quad r_{\Sigma\Xi}(^1S_0) = 4.00 \text{ fm},$$

$$a_{\Sigma\Xi}(^3S_1) = -1.90 \text{ fm}, \quad r_{\Sigma\Xi}(^3S_1) = 4.20 \text{ fm}.$$

#### D. $S = -3$ and $I = 1/2$ results

For ESC16, we obtained

$$a_{\Lambda\Xi^0}(^1S_0) = -0.56 \text{ fm}, \quad r_{\Lambda\Xi^0}(^1S_0) = 8.32 \text{ fm},$$

$$a_{\Lambda\Xi^0}(^3S_1) = +0.40 \text{ fm}, \quad r_{\Lambda\Xi^0}(^3S_1) = 2.52 \text{ fm}.$$

Around the  $\Sigma\Xi^0$  threshold, for  $I = 1/2$  states, we obtained the following:

$$\Sigma\Xi^0(^1S_0): A^{-1} = \begin{pmatrix} 31.537 & -29.454 \\ -29.454 & 34.928 \end{pmatrix},$$

$$R = \begin{pmatrix} 89.479 & 19.524 \\ 19.524 & -160.211 \end{pmatrix},$$

$$\Sigma\Xi^0(^3S_1): A^{-1} = \begin{pmatrix} 1.708 & 2.377 & 0.662 \\ 2.377 & 62.133 & -16.828 \\ 0.662 & -16.828 & 2.377 \end{pmatrix},$$

$$R = \begin{pmatrix} -0.208 & 13.675 & -3.522 \\ 13.675 & -472.466 & 98.143 \\ -3.522 & 98.143 & -15.637 \end{pmatrix}.$$

For ESC16\*(A), we obtained

$$a_{\Lambda\Xi^0}(^1S_0) = -1.147 \text{ fm}, \quad r_{\Lambda\Xi^0}(^1S_0) = 4.849 \text{ fm},$$

$$a_{\Lambda\Xi^0}(^3S_1) = +0.088 \text{ fm}, \quad r_{\Lambda\Xi^0}(^3S_1) = 76.227 \text{ fm}.$$

Around the  $\Sigma\Xi^0$  threshold, for  $I = 1/2$  states, we obtained

$$\Sigma\Xi^0(^1S_0): A^{-1} = \begin{pmatrix} 6.641 & 2.230 \\ 2.230 & -1.110 \end{pmatrix},$$

$$R = \begin{pmatrix} -18.459 & 10.465 \\ 10.465 & 2.826 \end{pmatrix},$$

$$\Sigma\Xi^0(^3S_1): A^{-1} = \begin{pmatrix} 2.750 & 6.882 & -0.150 \\ 6.882 & -89.577 & 2.952 \\ -0.150 & 2.952 & -0.267 \end{pmatrix},$$

$$R = \begin{pmatrix} -0.410 & 17.883 & -2.294 \\ 17.883 & -312.978 & 45.798 \\ -2.294 & 45.798 & -3.493 \end{pmatrix}.$$

For ESC16\*(B), we obtained

$$a_{\Lambda\Xi^0}(^1S_0) = -1.382 \text{ fm}, \quad r_{\Lambda\Xi^0}(^1S_0) = 4.342 \text{ fm},$$

$$a_{\Lambda\Xi^0}(^3S_1) = +0.002 \text{ fm}, \quad r_{\Lambda\Xi^0}(^3S_1) = 1.079 * 10^2 \text{ fm}.$$

Around the  $\Sigma\Xi^0$  threshold, for  $I = 1/2$  states, we obtained

$$\Sigma\Xi^0(^1S_0): A^{-1} = \begin{pmatrix} 8.826 & 1.680 \\ 1.680 & -0.569 \end{pmatrix},$$

$$R = \begin{pmatrix} -14.077 & 9.210 \\ 9.210 & 2.375 \end{pmatrix},$$

$$\Sigma\Xi^0(^3S_1): A^{-1} = \begin{pmatrix} 3.018 & 6.448 & -0.004 \\ 6.448 & -61.994 & 0.131 \\ -0.004 & 0.131 & 0.210 \end{pmatrix},$$

$$R = \begin{pmatrix} 0.648 & 5.124 & -0.729 \\ 5.124 & -232.352 & 34.303 \\ -0.729 & 34.303 & -2.321 \end{pmatrix}.$$

#### E. Bound states in $S$ waves

The scattering lengths and effective ranges in both models show no sign of a bound state. In particular, this is the case for  $\Xi\Xi(^1S_0)$ , which shows a weaker attraction than in  $pp(^1S_0)$ , and similarly for  $\Xi\Xi(^3S_1)$ . The effective range formula for the pole position of a possible bound state in momentum space is

$$\kappa_{\pm} = (1 \pm \sqrt{1 - 2r/a})/r, \quad B_{\pm} = -\kappa_{\pm}^2/(2m_{\text{red}}),$$

where the momentum is  $p_{\pm} = i\kappa_{\pm}$ . The pole closest to the lowest threshold is given by  $\kappa_{-}$ , and (usually)  $\kappa_{+}$  is outside the region of the approximate validity of the effective-range formula, which for  $\Xi\Xi(^1S_0)$  gives  $\kappa_{-} < 0$ , meaning an antibound state, and  $\kappa_{+}$  is too large for the effective range expansion to be valid. In the case of  $\Xi\Xi(^3S_1)$  the root is imaginary, and so there is no bound state. (Apparently there is enough SU(3) symmetry breaking and R symmetry breaking to prevent a deuteronlike bound state in this channel.) Similar analysis shows that also in the other channels bound states do not occur.

A discussion of the possible bound states, using the SU(3) content of the different  $S = 0, -1$ , and  $-2$  channels is given in Ref. [31]. In contrast to the NSC97 models, we find no  $S < 0$  bound states in the ESC16 models.

#### F. Partial-wave-phase parameters

For the  $BB$  channels below the inelastic threshold we use for the parametrization of the amplitudes the standard nuclear-bar phase shifts [38]. The information on the elastic amplitudes above thresholds is most conveniently given using the BKS phases [39–42]. For uncoupled partial waves, the elastic  $BB$   $S$ -matrix element is parametrized as

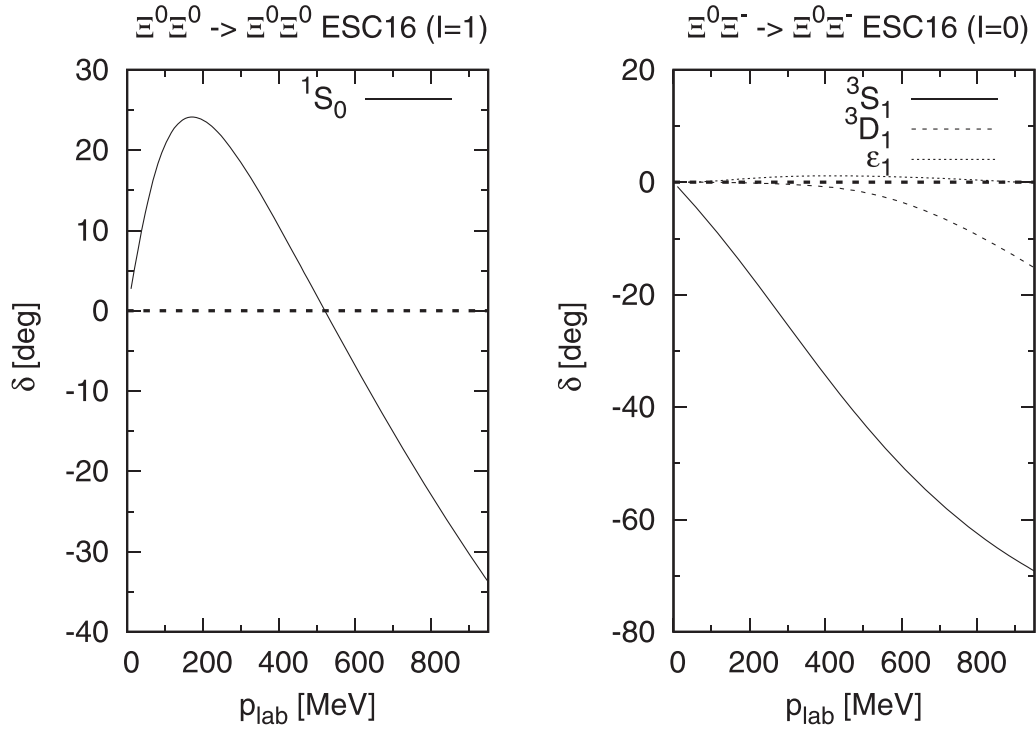
$$S = \eta e^{2i\delta}, \quad \eta = \cos(2\rho). \quad (5.1)$$

For coupled partial waves the elastic  $BB$  amplitudes are  $2 \times 2$  matrices. The BKS  $S$ -matrix parametrization reads

$$S = e^{i\delta} e^{i\epsilon} N e^{i\epsilon} e^{i\delta}, \quad (5.2)$$

where

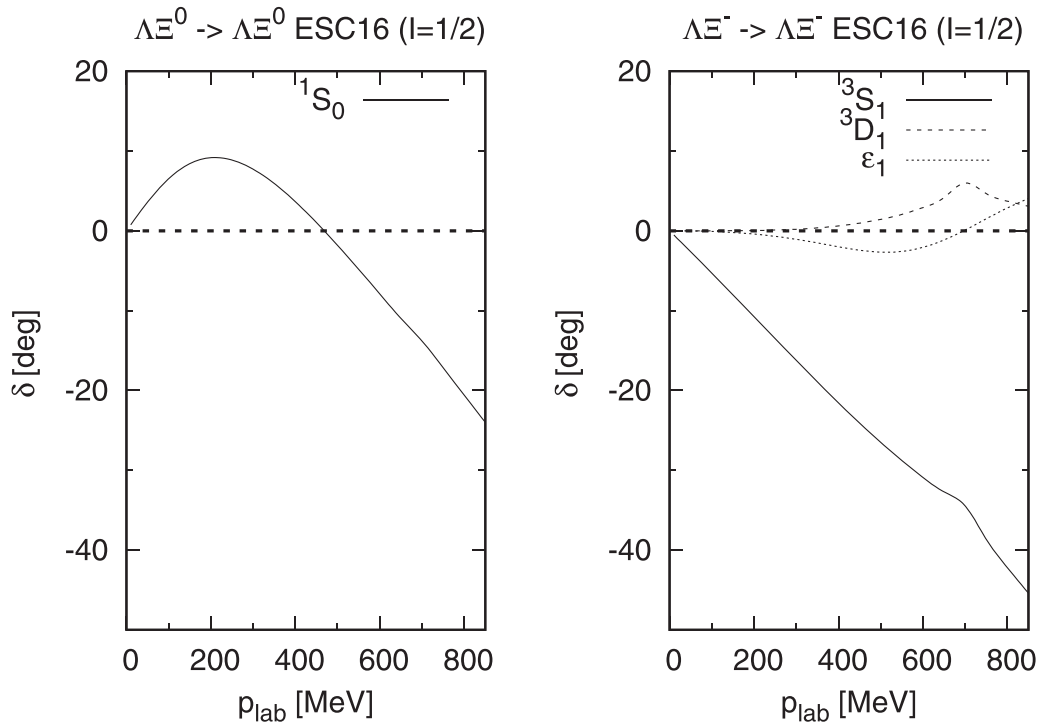
$$\delta = \begin{pmatrix} \delta_{\alpha} & 0 \\ 0 & \delta_{\beta} \end{pmatrix}, \quad \epsilon = \begin{pmatrix} 0 & \epsilon \\ \epsilon & 0 \end{pmatrix}, \quad (5.3)$$

FIG. 2. ESC16  $\Xi^0\Xi^0(^1S_0, I=1)$  and  $\Xi^0\Xi^-(^3S_1, I=0)$  phases.

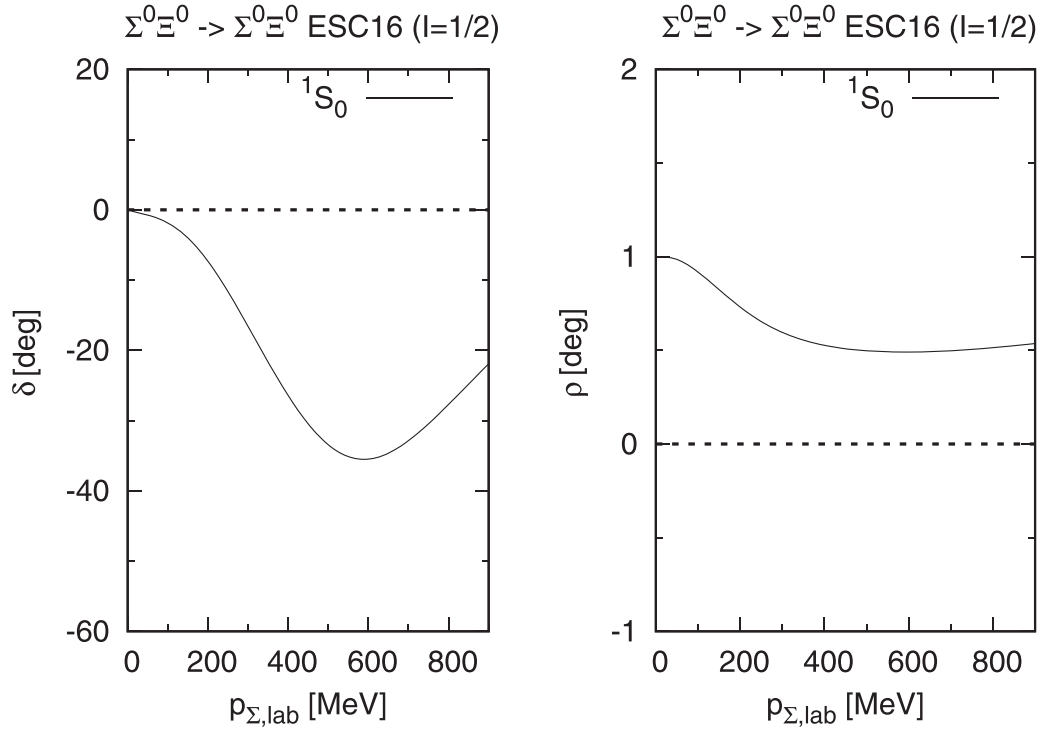
and  $N$  is a real, symmetric matrix parametrized as

$$N = \begin{pmatrix} \eta_{11} & \eta_{12} \\ \eta_{12} & \eta_{22} \end{pmatrix}. \quad (5.4)$$

In Fig. 2 the  $S = -4$  ESC16 nuclear-bar phases for  $\Xi^0\Xi^0(^1S_0, I=1)$  and  $\Xi^0\Xi^-(^3S_1, I=0)$  are shown. Figure 3 shows the  $\Lambda\Xi^0(^1S_0)$  and  $\Lambda\Xi^-(^3S_1 - ^3D_1)$  phase parameters. Figures 4 and 5 show for ESC16 the  $\Sigma^0\Xi^0(I=1/2)$  BKS

FIG. 3. ESC16  $\Lambda\Xi$   $I = 1/2$  phases.

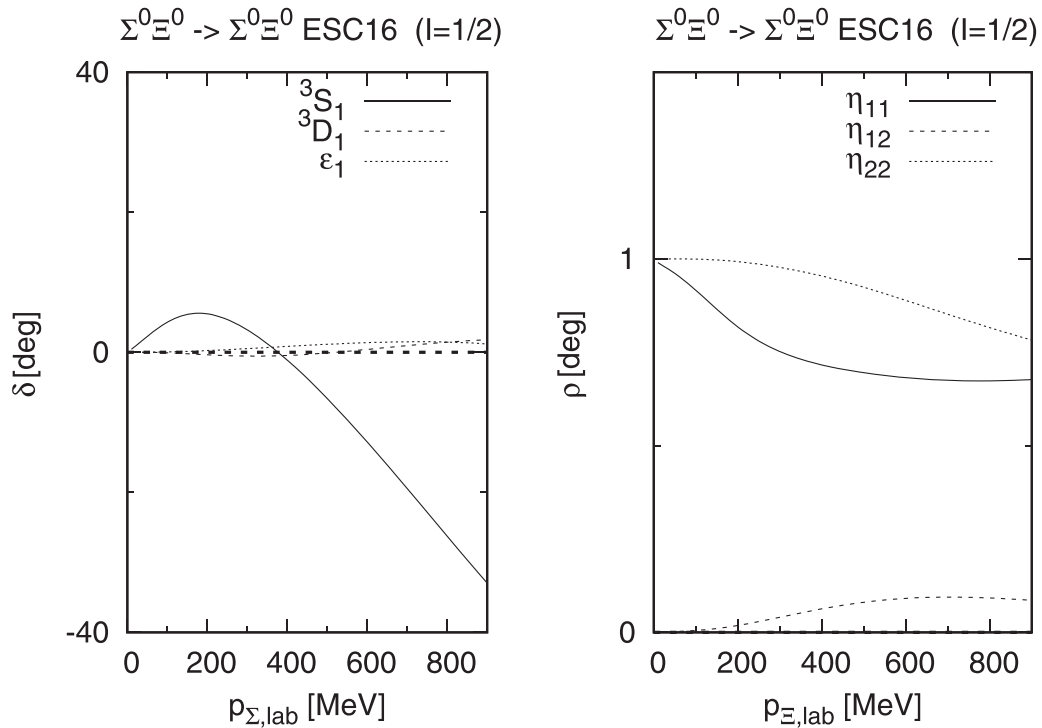


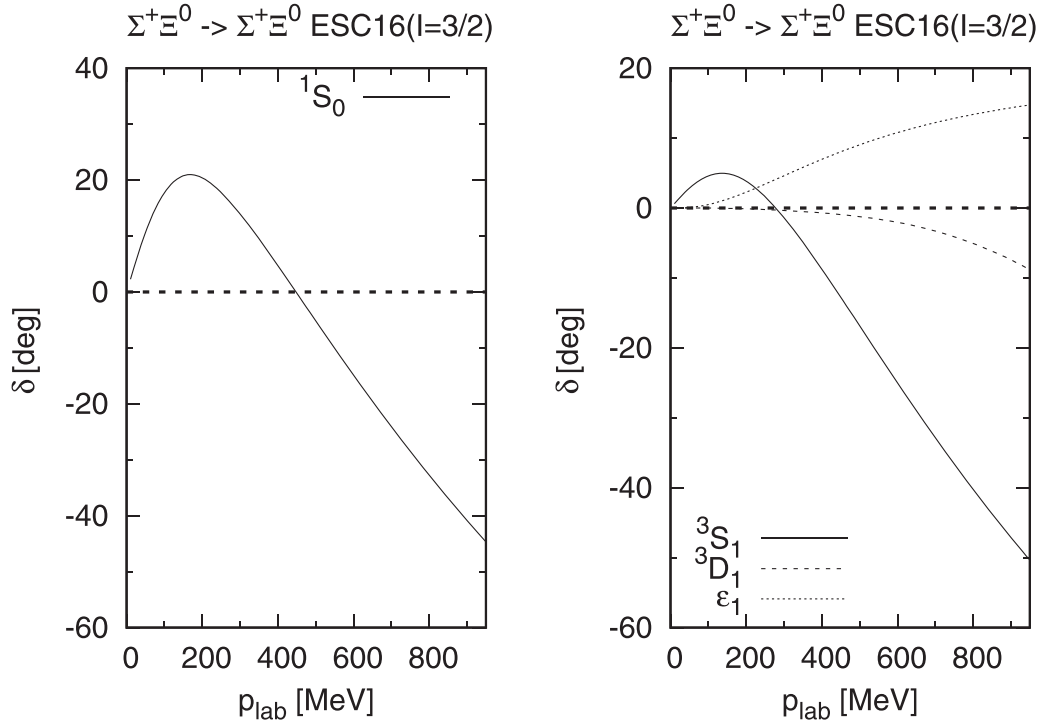
FIG. 4. ESC16  $I = 1/2$   $^1S_0(\Sigma^0\Xi^0)$  phases and  $\eta$  inelasticities.

phase shift and inelasticity parameters for  $^1S_0$  and  $^3S_1$ , respectively. Similarly, Fig. 6 shows the  $\Sigma^+\Xi^0(I = 3/2)$  phase shifts.

The  $\Xi^-\Xi^-$ ,  $\Xi^0\Xi^-$ , and  $\Xi^0\Xi^0$  nuclear-bar phase shifts for  $I = 1$  and  $I = 0$  as a function of the momentum and energy

are given in the tables in Appendix D for ESC16, as well as the results for the BKS parameters  $\Lambda\Xi^0$ ,  $\Lambda\Xi(I = 1/2)$ ,  $\Sigma\Xi^0(I = 1/2)$ , and  $\Sigma^+\Xi^0(I = 3/2)$ . The inelasticity parameters  $\rho$  and  $\eta_{11}$ ,  $\eta_{12}$ , and  $\eta_{22}$  contain the information to construct the  $\delta$ ,  $\epsilon$ ,  $N$ , and  $S$  matrices.

FIG. 5. ESC16  $I = 1/2$   $^3C_1(\Sigma^0\Xi^0)$  phases and  $\eta$  inelasticities.

FIG. 6. ESC16  $I = 3/2$   $\Sigma^+\Xi^0$  phases.

The  $\Xi\Xi(^1S_0, I = 1)$  phase shift is in agreement with LQCD (see Ref. [12], Fig. 2). For example, at  $p_{\text{lab}} = 200 \text{ MeV}/c$ , which means  $T_{\text{cm}} = 3.8 \text{ MeV}$ , ESC16 has  $\delta(^1S_0, I = 1) = 23.71^\circ$  (see Table XI), and ESC16\*(A) has  $\delta(^1S_0, I = 1) = 21.45^\circ$ , both of which match with the LQCD result.

Notice that the  $\Xi\Xi(^3S_1, I = 0)$  phase shows repulsion, except for very low energies. This means that the potential has a weak long-range attractive tail from one-pion-exchange. Qualitatively, this also agrees with the LQCD result.

## VI. DISCUSSION AND SUMMARY

An important result is that in the ESC16 models there is no bound state in the  $\Xi^0\Xi^0(I = 1, ^1S_0)$  channel, which is in the SU(3) irrep {27}. Since  $pp(^1S_0)$  and  $nn(^1S_0)$  are in the same irrep and quite attractive it might be expected naively that because of the larger  $\Xi$  mass a bound state might occur. Similarly, in the past sometimes it was speculated that a bound state could appear in  $\Sigma^+p$ . Apparently the breaking of SU(3) symmetry, due to using the physical meson and baryon masses, prevents such bound states.

It is seen from Fig. 2 and Table XII that  $\Xi^0\Xi^0(^1S_0)$  indicates an attractive interaction but this is weaker than in the case of, e.g.,  $\Sigma^+p$ . Also the preliminary data of the STAR Collaboration [14] indicate that the  $\Xi\Xi$  interaction in  $^1S_0$  is much weaker than that in  $pp$ .

To illustrate the basic properties of the potentials for  $S = -3$  and  $-4$  we have presented results for scattering lengths

and phase shifts in the tables. From these, the differential and total cross sections can be calculated easily. The results for the  $S = -3$  and  $-4$  channels of ESC16 and ESC16\*(A, B) are qualitatively similar. From Table I it is seen that the same SU(3) irreps occur in these channels as for  $S = 0$  and  $-1$ , where experimental data determine the interactions to a great extent.

Summarizing, the ESC16 and ESC16\*(A, B) models provide an SU(3)-based unified realistic description of all  $BB$  interactions, using single (OBE) and double (TME, MPE) meson-exchange potentials with Gaussian form factors. Here, the baryons are the SU(3) octet ground states with  $J^P = 1/2^+$ . The baryon-meson coupling constants can be systematically related to the quark-antiquark pair creation process with  $^3P_0$  dominance. Using (heavy) meson dominance this can be extended to the baryon-meson-pair couplings as well. The ESC potentials have been applied to calculate the properties of nuclei, hypernuclei, including double- $\Lambda$  and more exotic  $YY$  hypernuclei. Also, the interactions can be explored to study multiply strange systems and strange nuclear matter.

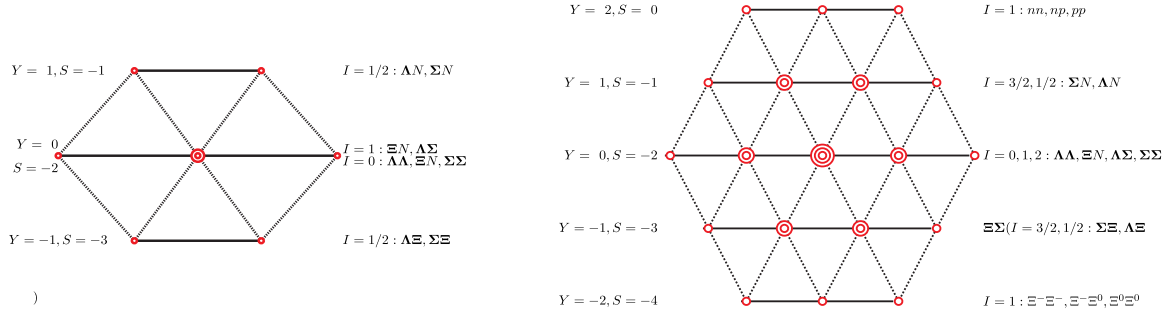
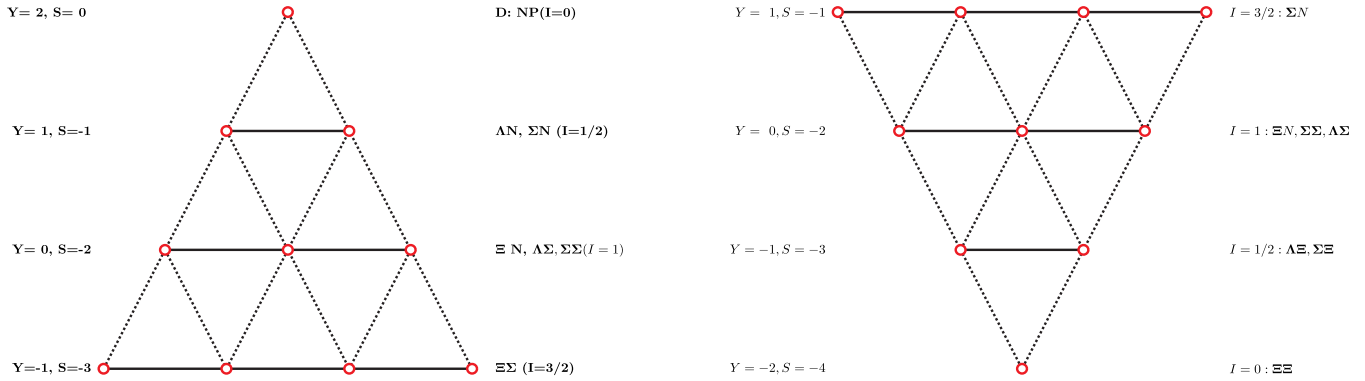
Application of the ESC interactions to the study of all  $\{8\} \otimes \{8\}$  two-baryon correlations measured in heavy-ion collision experiments is a future project, with the prospect of further insight into the low- and intermediate-energy baryon-baryon interactions.

## ACKNOWLEDGMENTS

Th.A.R. would like to thank P. M. M. Maessen and V. G. J. Stoks for their collaboration in constructing the soft-core  $S = -2, -3$ , and  $-4$  OBE model.

## APPENDIX A: SU(3) irreps AND BARYON-BARYON ISOSPIN STATES

The  $BB$  irreps are displayed in Figs. 7 and 8 showing the two-baryon content and the hypercharge  $Y = N + S$  of the SU(2) isospin multiplets.

FIG. 7. Baryon-baryon  $\{8\}$  and  $\{27\}$  states.FIG. 8. Baryon-baryon antidecuplet  $\{10^*\}$  and  $\{10\}$  states.

## APPENDIX B: MESON COUPLING CONSTANTS

In Tables VII and VIII the rationalized  $NNM$ ,  $YYM$ , and  $YNM$  OBE couplings are given for models ESC16 and ESC16\*, respectively. This is for pseudoscalar, vector, scalar, and axial-vector mesons.

TABLE VII. Coupling constants for model ESC16, divided by  $\sqrt{4\pi}$ .  $M$  refers to the meson. The coupling constants are listed in the order pseudoscalar, vector ( $g$  and  $f$ ), axial vector  $A$  ( $g$  and  $f$ ), scalar, axial vector  $B$ , and diffractive.

	$M$	$NNM$	$\Sigma\Sigma M$	$\Sigma\Lambda M$	$\Xi\Xi M$		$M$	$\Lambda NM$	$\Lambda\Xi M$	$\Sigma NM$	$\Sigma\Xi M$
$f$	$\pi$	0.2684	0.1955	0.1968	-0.0725	$K$	-0.2681	0.0713	0.0725	-0.2684	
$g$	$\rho$	0.5793	1.1586	0.0000	0.5793	$K^*$	-1.0034	1.0034	-0.5793	-0.5793	
$f$		3.7791	3.5185	2.3323	-0.2606		-4.2132	1.8810	0.2606	-3.7791	
$g$	$a_1$	-0.8172	-0.6260	-0.5822	0.1912	$K_{1A}$	0.8333	-0.2511	-0.1912	0.8172	
$f$		-1.6521	-1.2656	-1.1770	0.3865		1.6846	-0.5076	-0.3865	1.6521	
$g$	$a_0$	0.5393	1.0786	0.0000	0.5393	$\kappa$	-0.9341	0.9341	-0.5393	-0.5393	
$f$	$b_1$	-2.2598	-1.8078	-1.5656	0.4520	$K_{1B}$	2.3484	-0.7828	-0.4520	2.2598	
	$M$	$NNM$	$\Lambda\Lambda M$	$\Sigma\Sigma M$	$\Xi\Xi M$		$M$	$NNM$	$\Lambda\Lambda M$	$\Sigma\Sigma M$	$\Xi\Xi M$
$f$	$\eta$	0.1368	-0.1259	0.2599	-0.1958	$\eta'$	0.3181	0.3711	0.2933	0.3852	
$g$	$\omega$	3.1148	2.4820	2.4820	1.8492	$\phi$	-1.2384	-2.0171	-2.0171	-2.7958	
$f$		-0.5710	-3.2282	-0.2863	-4.4144		2.8878	-0.3819	3.2380	-1.8416	
$g$	$f'_1$	-0.7596	-0.1213	-1.0133	0.0710	$f_1$	0.5147	1.0503	0.3019	1.2117	
$f$		-4.4179	-3.1274	-4.9307	-2.7386		4.4754	5.5582	4.0450	5.8844	
$g$	$\varepsilon$	2.9773	2.3284	2.3284	1.6795	$f_0$	-1.5766	-2.2485	-2.2485	-2.9205	
$f$	$h'_1$	-1.2386	0.1171	-1.6905	0.5690	$h_1$	-0.0830	1.8346	-0.7222	2.4738	
$g$	$P$	2.7191	2.7191	2.7191	2.7197						
$g$	$O$	4.1637	4.1637	4.1637	4.1637						
$f$		-3.8859	-3.8859	-3.8859	-3.8859						

TABLE VIII. Coupling constants for model ESC16\*(A), divided by  $\sqrt{4\pi}$ .  $M$  refers to the meson. The coupling constants are listed in the order pseudoscalar, vector ( $g$  and  $f$ ), axial vector  $A$  ( $g$  and  $f$ ), scalar, axial vector  $B$ , and diffractive.

	$M$	$NNM$	$\Sigma\Sigma M$	$\Sigma\Lambda M$	$\Xi\Xi M$		$M$	$\Lambda NM$	$\Lambda\Xi M$	$\Sigma NM$	$\Sigma\Xi M$
$f$	$\pi$	0.2680	0.1978	0.1952	-0.0701	$K$	-0.2689	0.0737	0.0701	-0.2680	
$g$	$\rho$	0.5821	1.1641	0.0000	0.5821	$K^*$	-1.0082	1.0082	-0.5821	-0.5821	
$f$		3.7601	3.8215	2.1355	0.0614		-4.3773	2.2418	-0.0614	-3.7601	
$g$	$a_1$	-0.8526	-0.6681	-0.5988	0.1845	$K_{1A}$	0.8780	-0.2792	-0.1845	0.8526	
$f$		-3.1888	-2.4987	-2.2395	0.6902		3.2837	-1.0441	-0.6902	3.1888	
$g$	$a_0$	0.4905	0.8043	0.1019	0.3139	$\kappa$	-0.7575	0.6456	-0.3139	-0.4905	
$f$	$b_1$	-2.4303	-1.9442	-1.6837	0.4861	$K_{1B}$	2.5256	-0.8419	-0.4861	2.4303	
	$M$	$NNM$	$\Lambda\Lambda M$	$\Sigma\Sigma M$	$\Xi\Xi M$		$M$	$NNM$	$\Lambda\Lambda M$	$\Sigma\Sigma M$	$\Xi\Xi M$
$f$	$\eta$	0.1394	-0.1243	0.2584	-0.1966	$\eta'$	0.3181	0.3712	0.2941	0.3858	
$g$	$\omega$	3.0977	2.4618	2.4618	1.8260	$\phi$	-1.2183	-2.0007	-2.0007	-2.7831	
$f$		-0.5473	-3.3080	-0.6144	-4.7218		3.3335	-0.0634	3.2510	-1.8032	
$g$	$f'_1$	-0.7254	-0.0528	-0.9702	0.1611	$f_1$	0.4301	0.9945	0.2247	1.1739	
$f$		-4.8976	-2.3822	-5.8134	-1.5824		4.2124	6.3231	3.4440	6.9942	
$g$	$\varepsilon$	3.1268	2.6704	2.7949	2.2762	$f_0$	-1.5956	-2.1876	-2.0261	-2.6989	
$f$	$h'_1$	-1.2386	0.2194	-1.7246	0.7054	$h_1$	-0.1553	1.9069	-0.8428	2.5944	
$g$	$P$	2.8256	2.8256	2.8256	2.8256						
$g$	$O$	4.1637	4.1637	4.1637	4.1637						
$f$		-3.8859	-3.8859	-3.8859	-3.8859						

## APPENDIX C: MESON-PAIR COUPLING CONSTANTS

In Tables IX and X the rationalized  $NNM_p$ ,  $YYM_p$ , and  $YNM_p$  couplings are given for models ESC16 and ESC16\*, respectively. This is for scalar, vector, and axial-vector meson pairs  $M_p$ .

TABLE IX. Pair coupling constants for model ESC16, divided by  $\sqrt{4\pi}$ .  $I(M_p)$  refers to the isospin of the pair  $M_p$  with quantum numbers  $J^{PC}$ .

Pair	$J^{PC}$	Type	$I(M_p)$	$NNM_p$	$\Sigma\Sigma M_p$	$\Sigma\Lambda M_p$	$\Xi\Xi M_p$	$I(M_p)$	$\Lambda NM_p$	$\Lambda\Xi M_p$	$\Sigma NM_p$	$\Sigma\Xi M_p$
$\pi\eta$	$0^{++}$	$g$	1	-0.6881	-1.3763	0.0000	-0.6881	1/2	1.1919	-1.1919	0.6881	0.6881
			0	-1.1919	0.0000	0.0000	1.1919					
$\pi\pi$	$1^{--}$	$g$	1	0.2514	0.5028	0.0000	0.2514	1/2	-0.4354	0.4354	-0.2514	-0.2514
			0	0.4354	0.0000	0.0000	-0.4354					
$\pi\pi$	$1^{--}$	$f$	1	-1.7729	-1.4183	-1.2283	0.3546	1/2	1.8425	-0.6142	-0.3546	1.7729
			0	-0.6142	1.2283	-1.2283	1.8425					
$\pi\rho$	$1^{++}$	$g$	1	5.6913	4.5530	3.9431	-1.1383	1/2	-5.9147	1.9715	1.1383	-5.6913
			0	1.9715	-3.9431	3.9431	-5.9146					
$\pi\sigma$	$1^{++}$	$g$	1	-0.3892	-0.3114	-0.2697	0.0778	1/2	0.4045	-0.1348	-0.0778	0.3892
			0	-0.1348	0.2697	-0.2697	0.4045					
$\pi\omega$	$1^{+-}$	$g$	1	-0.3281	-0.2624	-0.2273	0.0656	1/2	0.3409	-0.1136	-0.0656	0.3281
			0	-0.1136	0.2273	-0.2273	0.3409					

TABLE X. Pair coupling constants for model ESC16\*(A), divided by  $\sqrt{4\pi}$ .  $I(M_p)$  refers to the isospin of the pair  $M_p$  with quantum numbers  $J^{PC}$ .

Pair	$J^{PC}$	Type	$I(M_p)$	$NNM_p$	$\Sigma\Sigma M_p$	$\Sigma\Lambda M_p$	$\Xi\Xi M_p$	$I(M_p)$	$\Lambda NM_p$	$\Lambda\Xi M_p$	$\Sigma NM_p$	$\Sigma\Xi M_p$
$\pi\eta$	$0^{++}$	$g$	1	-0.2683	-0.5365	0.0000	-0.2683	1/2	0.4646	-0.4646	0.2683	0.2683
			0	-0.4646	0.0000	0.0000	0.4646					
$\pi\pi$	$1^{--}$	$g$	1	0.2514	0.4071	0.0553	0.1557	1/2	-0.3802	0.3249	-0.1557	-0.2514
			0	0.3249	-0.0553	0.0553	-0.3802					
$\pi\pi$	$1^{--}$	$f$	1	-1.7729	-1.3973	-1.2404	0.3756	1/2	1.8303	-0.5899	-0.3756	1.7729
			0	-0.5899	1.2404	-1.2404	1.8303					
$\pi\rho$	$1^{++}$	$g$	1	5.8748	1.7084	5.7973	-4.1665	1/2	-4.3782	-1.4192	4.1665	-5.8748
			0	-1.4192	-5.7973	5.7973	-4.3782					
$\pi\sigma$	$1^{++}$	$g$	1	-0.3835	-0.1115	-0.3784	0.2720	1/2	0.2858	0.0926	-0.2720	0.3835
			0	0.0926	0.3784	-0.3784	0.2858					
$\pi\omega$	$1^{+-}$	$g$	1	-0.4364	-0.3491	-0.3023	0.0873	1/2	0.4535	-0.1512	-0.0873	0.4364
			0	-0.1512	0.3023	-0.3023	0.4535					



## APPENDIX D: ESC16 BKS PHASE PARAMETERS

The ESC16  $\Xi^- \Xi^-$  and  $\Xi^- \Xi^0$  nuclear-bar phase shifts as a function of energy are given in Table XII. The  $\Lambda \Xi$  BKS phase shifts and inelasticities are given in Tables XIII and XIV, respectively. Table XV shows the  $\Sigma^0 \Xi^0$  phase parameters, and Table XVI shows the  $I = 3/2$   $\Sigma^+ \Xi^0$  phases. Notice that the  $^3S_1$  phase shows repulsion, except for very low energies. This means that the potential has a weak long-range attractive tail.

TABLE XI. ESC16 nuclear-bar  $\Xi^- \Xi^- (I = 1, ^1S_0)$  and  $\Xi^0 \Xi^- (I = 0, ^3S_1)$  phases in degrees.

$p_\Lambda$ :	10	50	100	200	300	400	500	600
$T_{\text{lab}}$ :	0.038	0.95	3.77	15.05	36.63	59.22	91.94	129.85
$^1S_0$	0.04	7.01	17.27	23.71	19.43	11.69	3.05	-5.60
$^3S_1$	-0.75	-3.77	-7.72	-16.27	-25.36	-34.40	-42.86	-50.43
$\epsilon_1$	0.00	0.03	0.19	0.68	1.02	1.14	1.10	0.94
$^3P_0$	0.00	0.02	0.21	0.96	1.09	-0.53	-3.96	-8.63
$^1P_1$	0.00	0.02	0.24	1.64	3.76	15.21	5.13	3.51
$^3P_1$	-0.00	-0.00	-0.02	0.03	0.06	-0.51	-1.94	-4.11
$^3P_2$	0.00	0.01	0.10	0.68	1.31	1.14	-0.11	-2.20
$\epsilon_2$	-0.00	-0.00	-0.01	-0.07	-0.23	-0.47	-0.76	-1.07
$^3D_1$	-0.00	-0.00	-0.01	-0.13	-0.36	-0.80	-1.77	-3.543
$^1D_2$	0.00	0.00	0.01	0.16	0.74	1.95	3.66	5.49
$^3D_2$	0.00	0.00	0.03	0.31	0.93	1.66	2.16	2.18
$^3D_3$	0.00	0.00	0.00	0.04	0.20	0.40	0.37	-0.12

TABLE XII. ESC16 nuclear-bar  $\Xi^- \Xi^0$  phases in degrees.

$p_\Xi$ :	50	100	200	300	400	500	600	700	800	900
$T_{\text{lab}}$ :	0.95	3.80	15.12	33.79	59.50	91.86	130.42	174.72	224.24	278.51
$^1S_0$	12.65	20.69	23.73	18.44	10.44	1.77	-6.84	-15.11	-22.94	-30.28
$^3S_1$	-3.77	-7.72	-16.27	-25.36	-34.39	-42.85	-50.42	-56.98	-62.54	-67.19
$\epsilon_1$	0.03	0.19	0.68	1.02	1.14	1.10	0.94	0.70	0.40	0.05
$^3P_0$	0.04	0.25	0.99	0.99	-0.78	-4.32	-9.06	-14.41	-19.95	-25.41
$^1P_1$	0.04	0.31	1.78	3.88	5.23	5.03	3.31	0.45	-3.18	-7.29
$^3P_1$	-0.01	-0.02	0.03	0.03	-0.61	-2.10	-4.30	-6.933	-9.75	-12.57
$^3P_2$	0.02	0.13	0.73	1.32	1.09	-0.23	-2.35	-4.90	-7.61	-10.33
$\epsilon_2$	-0.00	-0.01	-0.08	-0.24	-0.48	-0.77	-1.07	-1.36	-1.60	-1.81
$^3D_1$	-0.00	-0.01	-0.13	-0.36	-0.80	-1.77	-3.54	-6.14	-9.42	-13.19
$^1D_2$	0.00	0.01	0.16	0.74	1.94	3.65	5.48	6.98	7.82	7.86
$^3D_2$	0.00	0.03	0.31	0.93	1.66	2.16	2.18	1.64	0.61	-0.77
$^3D_3$	0.00	0.00	0.04	0.20	0.40	0.37	-0.12	-1.11	-2.50	-4.12
$\epsilon_3$	0.00	0.00	0.04	0.15	0.29	0.40	0.48	0.52	0.53	0.51
$^3F_2$	0.00	0.00	0.01	0.07	0.21	0.42	0.55	0.43	-0.11	-1.16

TABLE XIII.  $I = 1/2$ : ESC16 nuclear-bar  $\Lambda \Xi^0$  phases in degrees.

$p_\Lambda$ :	10	50	150	250	350	450	550	650
$T_{\text{lab}}$ :	0.038	0.95	8.53	23.56	45.79	74.88	110.40	151.90
$^1S_0$	0.74	3.58	8.41	8.873	5.93	1.04	-4.82	-10.97
$^3S_1$	-0.53	-2.65	-8.02	-13.50	-18.94	-24.09	-28.78	-32.73
$\epsilon_1$	-0.00	-0.00	-0.12	-0.50	-1.26	-2.47	-4.20	-6.76
$^3P_0$	-0.00	-0.00	-0.06	-0.42	-1.42	-3.20	-5.64	-8.52
$^1P_1$	0.00	0.00	0.09	0.24	0.18	-0.32	-1.34	-2.80
$^3P_1$	-0.00	-0.00	-0.10	-0.47	-1.35	-2.79	-4.70	-6.85
$^3P_2$	0.00	0.00	-0.01	-0.15	-0.64	-1.59	-2.98	-4.68
$\epsilon_2$	-0.00	-0.00	-0.00	-0.01	-0.03	-0.06	-0.08	-0.09
$^3D_1$	0.00	0.00	0.01	0.09	0.36	0.96	2.05	4.15
$^1D_2$	0.00	0.00	0.01	0.10	0.41	1.04	1.99	3.20
$^3D_2$	-0.00	-0.00	-0.00	-0.00	-0.03	-0.14	-0.42	-0.87
$^3D_3$	-0.00	-0.00	-0.00	-0.01	-0.09	-0.35	-0.91	-1.80

TABLE XIV. ESC16  $^1S_0$ ,  $^3S_1 - ^3D_1$  ( $\Lambda \Xi \rightarrow \Lambda \Xi$ ,  $I = 1/2$ ) BKS-phase parameters in degrees as a function of the laboratory momentum  $p_\Lambda$  in MeV. The  $\Sigma^0 \Xi^0$  and  $\Sigma^+ \Xi^-$  thresholds are at  $p_\Lambda = 689.97$  MeV and  $p_\Lambda = 706.47$  MeV, respectively.

$p_\Lambda$	$\delta(^1S_0)$	$\rho(^1S_0)$	$\delta(^3S_1)$	$\epsilon_1$	$\delta(^3D_1)$	$\eta_{11}$	$\eta_{12}$	$\eta_{22}$
10	0.74	1.00	-0.53	-0.00	0.00	1.00	0.00	1.00
50	3.58	1.00	-2.65	-0.00	0.00	1.00	0.00	1.00
100	6.52	1.00	-5.31	-0.04	0.00	1.00	0.00	1.00
150	8.41	1.00	-8.02	-0.12	0.01	1.00	0.00	1.00
200	9.16	1.00	-10.75	-0.27	0.03	1.00	0.00	1.00
250	8.87	1.00	-13.50	-0.50	0.09	1.00	0.00	1.00
300	7.72	1.00	-16.24	-0.83	0.19	1.00	0.00	1.00
350	5.93	1.00	-18.94	-1.26	0.36	1.00	0.00	1.00
400	3.65	1.00	-21.56	-1.80	0.61	1.00	0.00	1.00
450	1.04	1.00	-24.09	-2.47	0.96	1.00	0.00	1.00
500	-1.82	1.00	-26.51	-3.26	1.43	1.00	0.00	1.00
550	-4.82	1.00	-28.78	-4.20	2.05	1.00	0.00	1.00
600	-7.90	1.00	-30.89	-5.32	2.90	1.00	0.00	1.00
650	-10.97	1.00	-32.73	-6.76	4.15	1.00	0.00	1.00
700	-13.80	0.990	-34.47	1.20	5.99	0.92	0.31	0.91
750	-17.14	0.972	-38.66	3.64	4.65	0.88	0.30	0.84
850	-23.997	0.956	-45.41	5.34	3.07	0.87	0.28	0.81
950	-30.624	0.945	-51.22	6.21	1.93	0.87	0.28	0.73
1050	-36.967	0.936	-56.42	6.69	0.70	0.87	0.28	0.71
1150	-42.966	0.928	-61.15	6.91	-0.70	0.88	0.28	0.68
1250	-41.319	0.921	-65.53	6.93	-2.26	0.89	0.29	0.66
1350	-35.927	0.915	-69.50	6.81	-4.06	0.89	0.29	0.64
1450	-30.988	0.908	-73.07	6.59	-5.96	0.90	0.29	0.64

TABLE XV. ESC16  $^1S_0$ ,  $^3S_1 - ^3D_1$  ( $\Sigma^0 \Xi^0 \rightarrow \Sigma^0 \Xi^0$ ,  $I = 1/2$ ) BKS-phase parameters in degrees as a function of the laboratory momentum  $p_\Sigma$  in MeV. The  $\Sigma^+ \Xi^-$  threshold at  $p_\Sigma = 138.15$  MeV.

$p_\Sigma$	$\delta(^1S_0)$	$\rho(^1S_0)$	$\delta(^3S_1)$	$\epsilon_1$	$\delta(^3D_1)$	$\eta_{11}$	$\eta_{12}$	$\eta_{22}$
10	-0.18	1.00	0.44	0.00	0.00	0.99	0.00	1.00
50	-0.85	1.00	2.19	0.01	0.00	0.96	0.00	1.00
100	-1.11	0.99	4.46	0.04	0.01	0.94	0.01	1.00
150	-2.38	0.83	8.14	-0.09	0.09	0.87	0.00	1.00
200	-3.65	0.67	7.38	-0.42	0.19	0.78	0.01	1.00
250	-10.02	0.59	6.01	-0.63	0.33	0.75	0.03	0.99
300	-16.30	0.55	4.24	-0.75	0.49	0.73	0.04	0.98
350	-22.32	0.52	2.12	-0.77	0.67	0.72	0.05	0.97
400	-28.05	0.50	-0.30	-0.69	0.86	0.71	0.07	0.96
450	-33.45	0.49	-2.99	-0.51	1.03	0.70	0.08	0.95
500	-38.52	0.48	-5.93	-0.27	1.20	0.69	0.09	0.93
550	-43.27	0.48	-9.07	0.04	1.34	0.68	0.09	0.91
600	-42.29	0.48	-12.37	0.37	1.46	0.68	0.10	0.89
650	-38.16	0.48	-15.81	0.72	1.56	0.67	0.10	0.87
700	-34.30	0.49	-19.32	1.04	1.64	0.67	0.10	0.85
750	-30.72	0.50	-22.85	1.34	1.68	0.67	0.10	0.83
850	-24.23	0.52	-29.86	1.78	1.63	0.67	0.09	0.80
950	-18.55	0.55	-36.59	2.05	1.28	0.68	0.08	0.76
1050	-13.51	0.58	-42.90	2.21	0.52	0.69	0.07	0.74
1150	-9.84	0.61	-48.69	2.30	-0.72	0.70	0.06	0.72
1250	-5.02	0.64	-53.98	2.39	-2.41	0.71	0.06	0.70
1350	-1.31	0.67	-58.93	2.51	-4.32	0.72	0.05	0.70
1450	1.94	0.70	-63.54	2.62	-6.62	0.74	0.04	0.69

TABLE XVI.  $I = 3/2$ : ESC16 nuclear-bar  $\Sigma^+ \Xi^0$  phases in degrees.

$p_{\Sigma^+}$	50	150	250	350	450	550	650	750	850	950
$T_{\text{lab}}$	1.05	9.42	25.99	50.43	82.28	121.01	166.03	216.72	272.51	332.83
$^1S_0$	12.15	22.97	19.53	10.95	1.04	-8.89	-18.41	-27.33	-35.62	-43.27
$^3S_1$	6.08	11.86	9.42	2.98	-4.90	-13.09	-21.11	-28.73	-35.86	-42.47
$\epsilon_1$	0.09	1.38	3.59	5.99	8.21	10.13	11.75	13.10	14.23	15.16
$^3P_0$	-0.07	-0.97	-2.63	-5.43	-9.75	-15.24	-21.33	-27.53	-33.52	-39.11
$^1P_1$	-0.07	-1.32	-4.55	-9.70	-16.21	-23.39	-30.68	-37.72	-44.28	-50.21
$^3P_1$	0.03	0.41	0.06	-1.69	-4.59	-8.15	-11.96	-15.78	-19.45	-22.90
$^3P_2$	0.01	0.04	-0.23	-1.31	-3.38	-6.19	-9.37	-12.67	-15.93	-19.08
$\epsilon_2$	0.00	0.07	0.20	0.20	0.06	-0.08	-0.15	-0.10	0.05	0.26
$^3D_1$	-0.00	-0.04	-0.20	-0.45	-0.81	-1.37	-2.22	-3.39	-5.29	-7.67
$^1D_2$	-0.00	-0.01	0.25	1.33	3.29	5.65	7.65	8.75	8.73	7.62
$^3D_2$	0.00	0.17	1.07	3.21	6.63	10.63	14.17	16.54	17.55	17.34
$^3D_3$	0.00	0.02	0.18	0.62	1.26	1.82	1.99	1.58	0.53	-1.11
$\epsilon_3$	0.00	0.01	0.11	0.32	0.69	1.23	1.90	2.65	3.44	4.27
$^3G_3$	-0.00	-0.00	-0.01	-0.03	-0.05	-0.03	0.08	0.31	0.72	1.35

[1] M. M. Nagels, Th. A. Rijken, and Y. Yamamoto, *Phys. Rev. C* **99**, 044002 (2019).

[2] M. M. Nagels, Th. A. Rijken, and Y. Yamamoto, *Phys. Rev. C* **99**, 044003 (2019).

[3] M. M. Nagels, Th. A. Rijken, and Y. Yamamoto, *Phys. Rev. C* **102**, 054003 (2020).

[4] V. G. J. Stoks and Th. A. Rijken, *Phys. Rev. C* **59**, 3009 (1999).

- [5] E. Hiyama, T. Motoba, and Y. Yamamoto, *Prog. Theor. Phys. Suppl.* **185**, 1 (2010).
- [6] S. Acharya *et al.* (ALICE Collaboration), *Phys. Lett. B* **797**, 134822 (2019); E. Hiyama, T. Motoba, and Y. Yamamoto, *Theor. Phys. Suppl.* **805**, 135419 (2020).
- [7] S. Acharya *et al.*, *Phys. Rev. Lett.* **123**, 112002 (2019).
- [8] L. Fabietti, V. Mantovani Sarti, and O. Vázquez Doce, *Annu. Rev. Nucl. Part. Sci.* **77**, 1 (2021).
- [9] T. Nagae, *Proceedings of APPC14*, Kuching, Malaysia, 17–22 November 2019.
- [10] Y. Fujiwara, Y. Suzuki, and C. Nakamoto, *Prog. Part. Nucl. Phys.* **58**, 439 (2007).
- [11] N. Ishii *et al.*, *PoS LATTICE2016*, 127 (2017).
- [12] T. Doi *et al.*, *arXiv:1702.01600*.
- [13] J. Haidenbauer and U.-G. Meissner, *arXiv:2201.08238*.
- [14] M. Isshiki, *EPJ Web Conf.* **259**, 11015 (2022).
- [15] H. Takahashi *et al.*, *Phys. Rev. Lett.* **87**, 212502 (2001).
- [16] M. Danysz *et al.*, *Nucl. Phys.* **49**, 121 (1963).
- [17] D. J. Prowse, *Phys. Rev. Lett.* **17**, 782 (1966).
- [18] E. Hiyama and K. Nakazawa, *Annu. Rev. Nucl. Part. Sci.* **68**, 131 (2018).
- [19] S. H. Hayakawa *et al.*, *Phys. Rev. Lett.* **126**, 062501 (2021).
- [20] M. Yoshimoto *et al.*, *Progr. Theor. Exp. Phys.* (2021) 073D02.
- [21] E. Hiyama, M. Isaka, T. Doi, and T. Hatsuda, *Phys. Rev. C* **106**, 064318 (2022).
- [22] Th. A. Rijken, *Phys. Rev. C* **73**, 044007 (2006).
- [23] Th. A. Rijken and Y. Yamamoto, *Phys. Rev. C* **73**, 044008 (2006).
- [24] A. Gal, E. V. Hungerford, and D. J. Millener, *Rev. Mod. Phys.* **88**, 035004 (2016); A. Gal, *AIP Conf. Proc.* **2130**, 020001 (2019).
- [25] L. Tolos and L. Fabietti, *Prog. Part. Nucl. Phys.* **112**, 103770 (2020).
- [26] S. Nishizaki, Y. Yamamoto, and T. Takatsuka, *Prog. Theor. Phys.* **105**, 607 (2001); **108**, 703 (2002).
- [27] R. L. Jaffe, *Phys. Rev. Lett.* **38**, 195 (1977); **38**, 617(E) (1977).
- [28] K. Nakazawa *et al.*, *Nucl. Phys. A* **835**, 207 (2010).
- [29] K. Nakazawa *et al.*, *Prog. Theor. Exp. Phys.* **2015**, 033D02 (2015).
- [30] T. Motoba and S. Sugimoto, *Nucl. Phys. A* **835**, 223 (2010).
- [31] Th. A. Rijken, V. G. J. Stoks, and Y. Yamamoto, *Phys. Rev. C* **59**, 21 (1999).
- [32] P. M. M. Maessen, Th. A. Rijken, and J. J. de Swart, *Phys. Rev. C* **40**, 2226 (1989).
- [33] M. M. Nagels, T. A. Rijken, and J. J. de Swart, *Ann. Phys.* **79**, 338 (1973).
- [34] J. J. de Swart, *Rev. Mod. Phys.* **35**, 916 (1963); **37**, 326(E) (1965).
- [35] M. Gell-Mann, Report CTSL–20, California Institute of Technology, 1961 (unpublished).
- [36] P. A. Carruthers, *Introduction to Unitary Symmetry* (Wiley & Sons, New York, 1966).
- [37] J. J. de Swart, M. M. Nagels, T. A. Rijken, and P. A. Verhoeven, Hyperon-nucleon interaction, in *Springer Tracts in Modern Physics*, edited by G. Höhler (Springer, Berlin, 1971), Vol. 60, p. 138.
- [38] H. P. Stapp, T. Ypsilantis, and N. Metropolis, *Phys. Rev.* **105**, 302 (1957).
- [39] R. A. Bryan, *Phys. Rev. C* **24**, 2659 (1981); **30**, 305 (1984).
- [40] S. Klarsfeld, *Phys. Lett. B* **126**, 148 (1983).
- [41] D. W. L. Sprung, *Phys. Rev. C* **32**, 699 (1985).
- [42] A. Kabir and M. W. Kermode, *J. Phys. G: Nucl. Phys.* **13**, 501 (1987).